Tunable coupling by means of oxygen intercalation and removal at the strongly interacting graphene/cobalt interface

Matteo Jugovac[a,1,*], Francesca Genuzio[b,*], Tevfik Onur Menteş[b], Andrea Locatelli[b], Giovanni Zamborlini[a,2], Vitaliy Feyer[a,c], Claus Michael Schneider[a,c]

[a] *Peter Grünberg Institute (PGI-6), Forschungszentrum Jülich GmbH, 52425 Jülich, Germany*
[b] *Elettra - Sincrotrone Trieste, S.S. 14 km 163.5 in AREA Science Park, Basovizza, I-34149 Trieste*
[c] *Fakultät f. Physik and Center for Nanointegration Duisburg-Essen (CENIDE), Universität Duisburg-Essen, D-47048 Duisburg, Germany*

Abstract

It is well known that intercalated species can strongly affect the graphene-substrate interaction. As repeatedly shown by experiment and theory, the intercalation of atomic species may establish a free-standing character in chemisorbed graphene systems. Here, we focus on graphene grown on a strongly interacting support, cobalt, and demonstrate that the film electronic structure and doping can be tuned via the intercalation/de-intercalation of interfacial oxygen. Importantly, cathode lens microscopy reveals the main mechanism of oxygen intercalation, highlighting the fundamental role of microscopic openings in graphene in oxygen enrichment at the graphene/cobalt interface. Our experiments show that this process can be carefully controlled through temperature, without affecting the film morphology and crystalline quality. The presence of oxygen at the interface induces an upward shift of the graphene π band, moving its crossing above the Fermi level, accompanied by an increased Fermi velocity and reduced momentum width. Control on the graphene coupling to cobalt may enable one to alter the induced spin polarization in graphenes electronic states.

1. Introduction

The usage of graphene in next-generation electronics demands an accurate control of the coupling between the film and the underlying support. This is particularly true for the case of metal electrodes where a controlled alignment of the electronic states and band-gap opening is required. Another relevant case is the spin-dependent electronic transport in graphene, where the spin polarization is induced by the proximity with a ferromagnetic support.

*Corresponding author
Email addresses: m.jugovac@fz-juelich.de (Matteo Jugovac), francesca.genuzio@elettra.eu (Francesca Genuzio)
[1] Present address: Istituto di Struttura della Materia-CNR (ISM-CNR), Trieste, 34149, Italy
[2] Present address: Technische Universität Dortmund, Experimentelle Physik VI, 44227 Dortmund, Germany

Among the various Gr/metal coupled systems, graphene/cobalt heterostacks are of significant interest in 2D magnetism. Compared to other ferromagnetic supports, such as Ni and Fe, ultrathin Co undergoes a graphene-induced spin reorientation transition from in-plane to out-of-plane, which has direct relevance for high-density data storage with reduced energy consumption. Another intriguing feature of Gr/Co is the presence of antisymmetric Dzyaloshinskii-Moriya exchange interaction (DMI) when such ultrathin heterostacks are supported on particular heavy metal substrates. As a consequence, the occurrence of chiral domain walls foresee the stabilization of skyrmions or other topologically-protected magnetic structures to be used for high processing speed in next-generation spintronic devices.

In this context, the manipulation of the interface structure is a pathway to control the electronic interaction at the interface, and hence a possible way to tune the magnetic properties of the Gr/Co heterostack. Intercalation of foreign atoms and molecules, for instance O_2, H_2, H_2O and CO, provides an established method to decouple graphene from the substrate. Such decoupling is most frequently accompanied by a notable modification of the graphene electronic structure, as has been demonstrated for the case of graphene on various transition metals, *e.g.* Ir, Ru, Ni, Cu [1, 2, 3, 4, 5]. In this respect, the intercalation of oxygen has attracted considerable interest, as it may find application in graphene transfer methods [6], graphene doping [1, 7, 8, 9] and catalysis in confined spaces [8, 10, 11]. In a few cases, the intercalation process has proven to be reversible [9, 12]. From the point of view of chemical kinetics, the intercalation is a spatially heterogeneous process. In the case that the graphene film is physisorbed on the substrate, the intercalation and diffusion of the adspecies are facilitated by a large graphene-substrate separation and their relatively weak interaction [8, 4]. Instead, for strongly-interacting substrates the penetration of adatoms through the graphene layer is thought to occur at defects in the graphene lattice, such as vacancies or grain boundaries. Therefore, elucidating the underlying mechanisms related to the lateral heterogeneity of the graphene layer is of importance.

Along these lines, the current study focus on the intercalation/de-intercalation of oxygen at the graphene-cobalt interface with emphasis on the role of heterogeneities within the graphene layer. The interest in this system derives from the possibility to modify spin-dependent interaction occurring between graphene and cobalt. It has been recently demonstrated that the strong coupling at the graphene-cobalt interface induces a pronounced spin-polarization in graphene band features close to the Fermi level (termed in the literature as the *minicone states*) [13, 14, 15, 16, 17]. Thus, shifts in the graphene electronic bands induced by intercalated species offer a means to control the spin-polarization in the graphene states. Moreover, such changes are expected to also affect the magnetic properties of the ferromagnetic support itself, most importantly regarding the enhanced perpendicular magnetic anisotropy (PMA) in ultra-thin Co films induced by graphene [18, 19, 20, 21, 22]. In particular, by suppressing (or restoring) the hybridization between Gr and substrate atoms, the intercalation of oxygen can change the magnetic anisotropy of cobalt, which may find application in sensors and devices.

Despite the large number of works addressing the intercalation of exo-species under graphene, the case of graphene-Co and oxygen has been the subject of only one study to date [23]. Here, we present a microscopy investigation of oxygen intercalation in graphene/Co and its relevance on graphenes electronic properties. We employ a set of methods based on cathode lens microscopy, namely Low Energy Electron Microscopy

(LEEM) and X-ray Photoemission Electron Microscopy (XPEEM) for the characterization of oxygen intercalation at the graphene/cobalt interface and its relation to the lateral heterogeneity found in the graphene layer. This is followed by the investigation of the oxygen-induced effects on the electronic structure of the system performed using synchrotron-based k-resolved PhotoEmission Electron Microscopy (k-PEEM). The last part of the manuscript treats the reversibility of the intercalation process, such that the properties of the pristine graphene/cobalt system can be restored, thus allowing for intercalation/deintercalation cycles.

2. Methods

All experiments were performed at the Nanospectroscopy (SPELEEM) [24] and NanoESCA (PEEM) [25] experimental end-stations of the Elettra storage ring (Trieste, Italy), located at the same beamline. The beamline provides soft X-rays in the energy range 25-1000 eV, with tunable elliptical and linear polarization.

The LEEM and XPEEM experiments were carried out using the Spectroscopic Photoemission and Low Energy Electron Microscope (SPELEEM). This instrument combines Low Energy Electron Microscopy (LEEM) and Diffraction (LEED) with X-ray Photo-Emission Electron Microscopy (X-PEEM). In LEEM, the contrast between different surface regions arises from differences in the elastic backscattering cross-sections of low energy electrons, and it is specific for different surface phases (both from chemical and structural point of view). The electron energy is chosen by applying a voltage bias to the sample, commonly known as start voltage, V_{st}. LEEM microscopy allows one to image the specimen surface at video frame rate and hence can be employed for real-time imaging of dynamical processes at surfaces (lateral resolution better than 15 nm). In X-PEEM mode, the image contrast originates from local variations in the photoemission intensity, which is associated with the presence of distinct chemical species. By scanning the energies across relevant core level energies, XPEEM allows to characterize the chemical composition of the surface, with high lateral resolution (less then 30 nm) being exploited to perform laterally resolved XPS in imaging mode.

The NanoESCA endstation hosts a electrostatic PEEM equipped with a double-pass hemispherical analyzer (Focus GmBH/Omicron NanoESCA II). By proper tuning of the lenses, the instrument can operate in both real and reciprocal space mode. The instrument, in reciprocal space mode operation, is capable of detecting angle-resolved photoemission intensities in the full-emission hemisphere above the sample surface. This operation mode allows the acquisition of 2D momentum maps at selected kinetic energy. By changing the electron kinetic energy, the E *vs.* k data cube can be obtained, with parallel momentum varying in the [-2; 2] Å range. From the 3D stack of images, the momentum maps along arbitrarily chosen directions can be extracted. The data were collected using p-polarized light at a photon energy of 56 eV; in the geometry of our set-up, the polarization vector forms an angle of 65° with the sample surface. The energy and momentum resolutions were 75 meV and 0.05 Å, respectively. The binding energy scale is referred to as bare Co Fermi edge.

The samples were prepared by depositing cobalt from a high purity rod (99.995%) using an e-beam evaporator. A W(110) single crystal was chosen as substrate, which favors Co epitaxial growth. The deposition was carried out keeping the sample at room

temperature until a thickness of about 10 nm was reached. The samples were post annealed in UHV, which improved the crystalline quality of the film, as verified by LEED. Graphene was grown by ethylene CVD, by backfilling the experimental chamber with ethylene (2-4·10^{-6} mbar range) while keeping the sample at about 500 °C. This treatment leads to the formation of rotationally incoherent graphene, which was transformed into an epitaxial layer during subsequent annealing to higher temperatures, as detailed in ref. [26]. The oxygen intercalation at the Gr/Co interface was obtained by exposing the surface to molecular oxygen (p = 5·10^{-6} mbar) at a temperature of about 200-220 °C. The values of oxygen exposure in the manuscript are given in Langmuirs (1 L = 1.33·10^{-6} mbar·s). All preparation steps and the intercalation process were monitored in real time using LEEM; XPEEM was used for the spatially resolved chemical characterization of the sample. The electronic structure was investigated using momentum-resolved photoemission spectroscopy.

3. Results and discussion

Graphene was grown by CVD of C_2H_4 at T ≈ 500 °C, resulting in the formation of a film with rotational domains oriented at about 20° with respect to the Co high symmetry directions [14] (indicated as R20 in the following). Subsequently, graphene was transformed into an epitaxial layer (R0). The transformation between the two graphene orientations occurs through a recrystallization process assisted by the dissolution of carbon in the topmost Co surface layer. The process is described in detail in ref. [27, 26]. Notably, the transformation to epitaxial graphene (bright regions in Fig. 1a) leaves a residual coverage of R20 islands (light gray contrast) plus few holes in the graphene film (dark regions in Fig. 1). Here, cobalt carbides are formed [26]. We found that the size and the number of the carbidic holes can be controlled by tuning the p/T ratio during CVD. For our preparation conditions, we estimate that the carbidic holes cover about 5% of the surface, see Figure 1a.

We did not observe oxygen intercalation at RT even upon exposure to ambient pressure, proving the efficiency of graphene as a protective barrier against oxidation. The intercalation of oxygen below graphene is known to be a thermally activated process, occurring in the temperature range between 200 and 400 °C. In our preparations, exposure to molecular oxygen was thus carried out in the 200-250 °C temperature range, being well below 450 °C, in order to prevent graphene etching by reaction with atomic oxygen. Under these conditions we found that the intercalation starts after about 200 L O_2 exposure, as illustrated by the LEEM images in Fig. 1. Here, the growing regions where oxygen has intercalated appear neutral grey. The change of image contrast, caused by the local variation of the electron reflectivity, indicates the formation of a different surface phase. We note that the intercalation front initiates in the proximity of the carbidic regions, *i.e.* holes in the graphene layer (Fig. 1b) and then propagates (Fig. 1c-e) following the step morphology of the cobalt film (visible in LEEM such as steps and grain boundaries). In the regions of epitaxial graphene without carbidic holes, the spontaneous intercalation points, defined as spatial regions where local oxygen enrichment occurs at the interface, are absent. Considering that, together with the presence of clear intercalation fronts, suggests that the intercalation mainly obeys the edge-limiting mechanism [7]. A different behavior is observed in the R20 region. The start of oxygen accumulation underneath these rotated regions depends on the relative distance from the

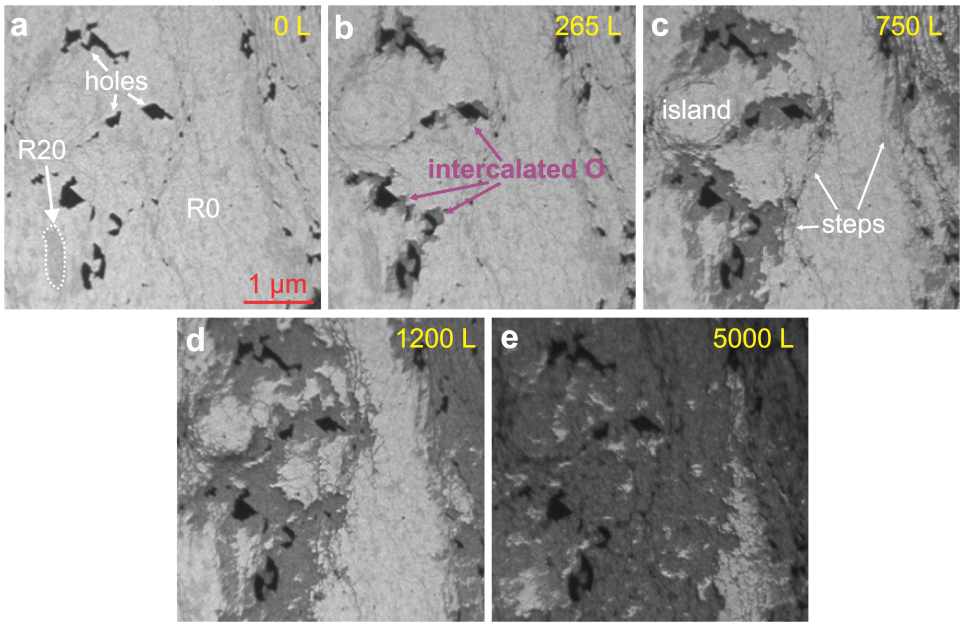

Figure 1: Series of LEEM images (V_{st}= 13 V) showing the intercalation during O_2 exposure (p = $5{\cdot}10^{-6}$ mbar) at T = 220 °C. a) As prepared surface, consisting of epitaxial (bright), rotational Gr/Co domains (light gray) and holes in the layer visible (dark). b-d) Sequence of images showing the intercalation process. The intercalated and non-intercalated (pristine) areas have dark gray and bright contrast, respectively. O_2 dose is indicated in the images. e) Surface after the exposure of 5000 L (corresponding to about 62') O_2 at 220 °C.

carbidic intercalation centers. This allows us to exclude the influence of grain boundaries as intercalation centers. However, once started (Fig. 1), the intercalation under the R20 domains appears to proceed faster as compared to the R0 ones. This observation is in line with the work by Bignardi *et al.* [12] and by Vlaic *et al.* [28] (O_2 intercalation in Gr/Ni and Co intercalation in Gr/Ir(111) respectively) and is an indication that the energy barrier for O_2 diffusion at the interface is smaller for the rotated phase. We remark that in a sample fully composed by misoriented graphene domains and absent of carbidic islands, oxygen accumulation was not observed even after about 5000 L of oxygen exposure.

As seen in Fig. 1e, after dosing 10000 L of oxygen, about 20% of the surface remains non-intercalated; this value varies across the sample depending on the local morphology of the graphene/Co interface (R0 and R20) as well as on the density of the carbidic islands. In our experiment, we have found that the non-intercalated regions lie exclusively in the R0 phase, and these regions do not contain carbidic holes. These facts support the idea that the rate-limiting step of the process occurs at the intercalation front itself.
The possible limiting steps are two: i) the detachment of the edge carbon atoms from the metal, as in the case for gr/Ru(0001) by Sutter *et al.* [8]; ii) the diffusion of adsorbed O atoms through the edge of the graphene/metal interface, where the C-M bond is broken and the dangling bonds passivated by oxygen atoms [7].

The intercalation rate observed in our experiment is estimated to be 0.1 μm^2/s, which was obtained by measuring the time-dependent propagation of the intercalated area visible in Fig. 1. This value can allow us to estimate the activation energy for the intercalation of oxygen in Gr/ Co, as described in detail in the Supporting Information. The energy barrier for Gr/O/Co is about 0.4 eV, close to that found for the Gr/O/Ru(0001) system [8].

The intercalation manifests with the rise of the O *1s* signal in the XPS spectrum (Fig. 2a). We identify a single O *1s* peak at E_B = 529.5 eV, characteristic of chemisorbed atomic oxygen [29, 30], therefore excluding the formation of cobalt oxide species. XPEEM at the O *1s* core level (Fig. 2c) highlights that the oxygen is inhomogeneously distributed across the surface. The highest oxygen concentration is found at the carbidic holes of the graphene layer (region C in Fig. 2c). The O *1s* photoemission signal from the non-intercalated regions is below the instrumental detection limit, meaning that the intercalation is restricted to the oxygen diffusion front. Therefore, the underlying mechanism proceeds through oxygen adsorption and decomposition at the carbidic islands, which act as atomic oxygen supply, allowing for its accumulation under the graphene layer. The absence of the O *1s* signal in the non-intercalated regions means that the epitaxial graphene layer itself is impermeable to O_2.

The C *1s* core level spectrum (Fig. 2b) exhibits significant changes upon oxygen intercalation. The C *1s* component at a binding energy of 285.05 eV, attributed to strongly interacting graphene, shifts by 1.1 eV towards lower binding energy (E_B= 283.95 ev), as expected in the case of graphene decoupled from its support. The marked binding energy shift upon the presence of oxygen indicates the suppression of the charge transfer between the graphene and the metal substrate (quasi-free-standing graphene) [1, 2, 5, 9, 31]. The fitted peak area is identical to that of the pristine regions and is unchanged with respect to the sample before intercalation. Thus, we can conclude that the amount of C possibly removed during the oxygen intercalation is below the XPS detection limit. In addition to the core-level shift, the work function of the system also changes upon

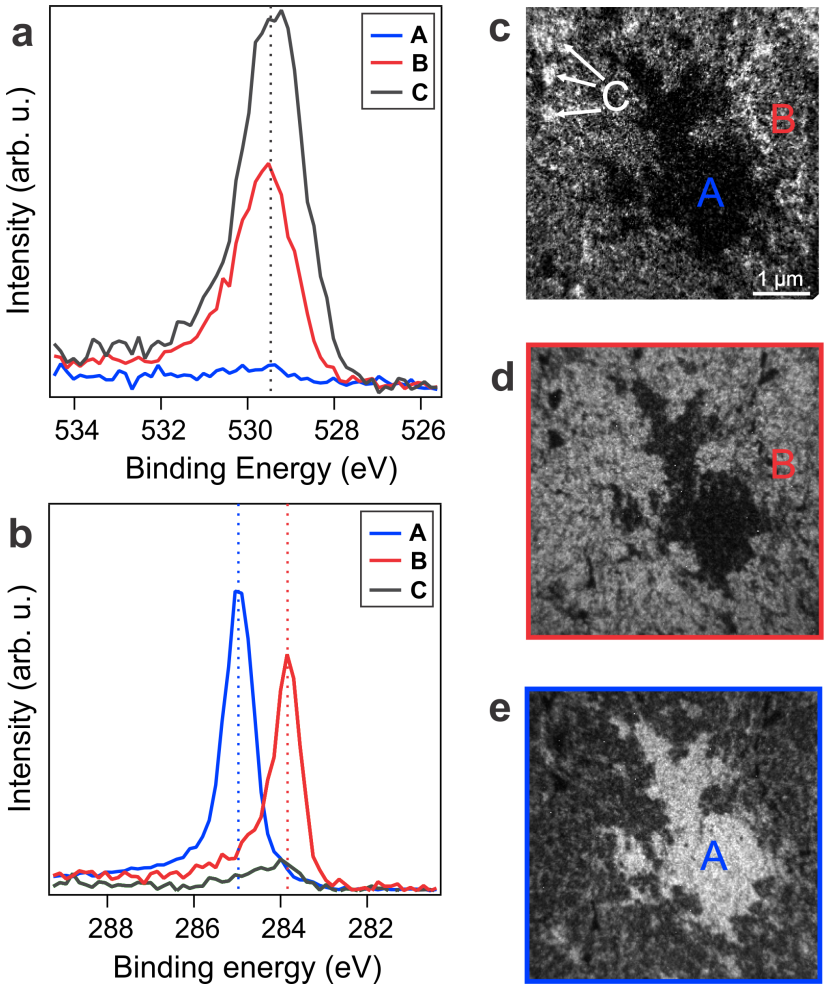

Figure 2: a,c) Local spectra and XPEEM image at the O *1s* core level (hν = 650 eV) acquired after intercalation, evidencing the inhomogeneous O enrichment: for non-intercalated regions (A), intercalated areas (B) and O-rich areas (C) located close to the holes (*i.e.* the intercalation starting points). b) Local spectra at the C *1s* core level (hν = 400 eV) for the pristine (not intercalated) regions (A) and intercalated regions (B); intercalated regions show a peak shifted by 1 eV to lower binding energy. d,e) XPEEM images acquired in the C *1s* region (at binding energies as indicated in the images) at the non-interacting peak (d) and at the interacting peak (e). The two images are characterized by a clear inversion of contrast.

intercalation, with a value 0.85 eV higher with respect to the pristine case.

By comparing the O *1s* and C *1s* peak intensity, accounting for the attenuation lengths, damping and photoionization cross-sections, we find the oxygen/carbon ratio to be approximatively 1:4. This ratio can be justified by the formation of a p(2x2)-2O structure, characterized by an oxygen coverage of 0.5 ML [32]. At this coverage, the most stable structure features a unit cell composed by an oxygen atom in the *fcc* and one in *hcp* site, according to ref. [32].

On the contrary to what has been observed upon oxygen intercalation at TM/graphene interfaces, where oxidation of the metal support occurs [1, 33], we exclude oxidation of the Co substrate under these conditions based on the Co *3p* XPS, the valence band spectrum in normal emission and the XAS at the Co $L_{2,3}$. In all the spectra, we confirm the absence of the typical oxide fingerprint. Moreover, we performed X-ray Magnetic Circular Dichroism (XMCD) measurements at the Co $L_{2,3}$ edge in remanent magnetization (see Supporting Information). The analysis of the spectra reveals that the ferromagnetic character of the cobalt substrate is preserved after intercalation. Using the well-known sum rules [34, 35], and a number of *3d* holes of 2.9, we determined the values of the magnetic moments. The extracted value of the orbital moment $\mu_L = 0.18\mu_B$ and of the spin moment $\mu_S = 1.47\mu_B$ are in agreement with the values determined for a cobalt thin film under graphene [36]. This fact is of fundamental importance when considering cobalt as a building block for the realization of spintronic devices. We remark that the presence of the oxygen atoms in between the Co and the Gr causes the damping of the Co-related features in all spectra from the intercalated regions.

In order to get an insight into the effects of oxygen intercalation on the electronic structure, momentum mapping in the valence band has been performed. The momentum maps from the oxygen intercalated Gr/Co are compared to the experimentally found band structure of the Gr/Co measured before intercalation. As previously reported [14, 16], the interaction of graphene with Co leads to the formation of two Dirac-like features (Fig. 3a), one at high binding energy and a second one at the Fermi level (mini-cone, following the nomenclature introduced by Usachov *et al.* [14]). The strong hybridization of the substrate *d* states with p_z orbitals of graphene atoms shifts the graphene π band to higher binding energies, as visible in Fig. 3a. The graphene-related features in the momentum distribution curves (MDCs), acquired along the ΓK direction, were fitted with two Lorentzian profiles between $E_B = 5.1$ eV and $E_B = 3$ eV. The interpolation of the Lorentzian maxima with a linear fit allowed us to estimate that the Dirac point is positioned at $E_B = 2.83\pm0.04$ eV, while the value of the Fermi velocity (v_F) is found to be $1.01\cdot10^6$ m/s, in agreement with [14].

Oxygen intercalation dramatically alters the electronic structure, as shown in Fig. 3b. The main Dirac cone is shifted upwards while we note the disappearance of the mini-cone feature. The shifting of the main Dirac cone originates from the lifting of the graphene π and cobalt *d* band hybridization, leading to an upward translation of the graphene π band, whose crossing at K point is 0.43 ± 0.03 eV above the Fermi level, indicating hole doping of the graphene layer as expected from the presence of the oxygen. The position of the Dirac cone apex in this case is found at slightly lower binding energy values with respect to similar TM/O_2/graphene interfaces: 0.55 eV for Ru(0001) [37], 0.80 eV/0.57 eV for Ir(111) [38, 2], 0.63 for Rh(111) [39] and 0.35 for Cu(111) [9]. Moreover, upon intercalation, the Fermi velocity increases by about 9% ($v_F = 1.09\cdot10^6$m/s), becoming closer to that of the free-standing graphene layer [40].

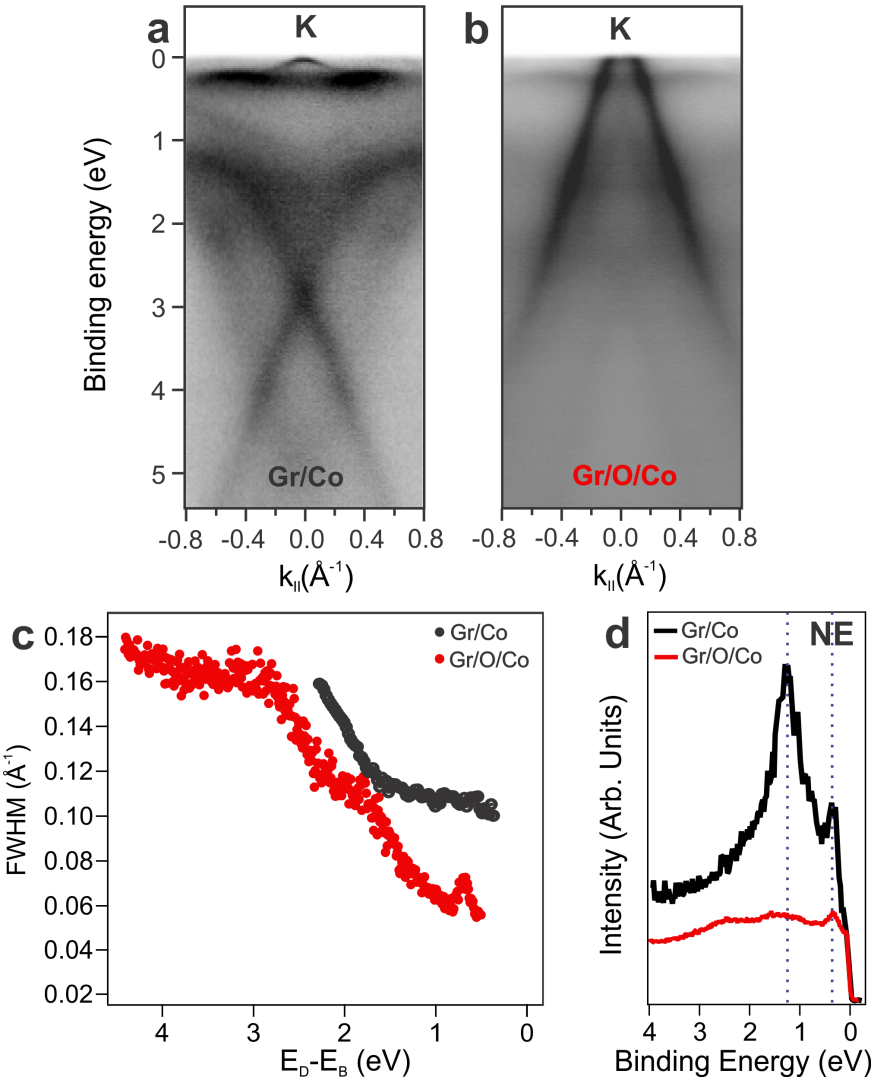

Figure 3: a) Momentum map acquired along ΓK direction and centered at the K point of: a) pristine Gr/Co interface b) fully oxygen intercalated region. c) Energy dependence of the momentum width of the graphene related features in the electronic structure. E_D - E_B indicates the binding energy with respect to the Dirac point in the two distinct cases (a) and b)). d) VB photoemission spectra acquired in normal emission of the two phases listed above. All spectra were acquired at -140 °C, using p-polarized photons as excitation source of hν = 56 eV.

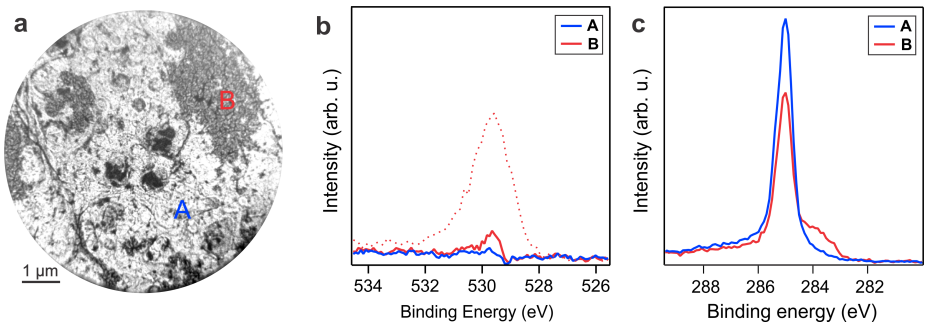

Figure 4: Sample surface comprising pristine (A) and intercalated regions (B) after UHV annealing (T = 420 °C) and O_2 deintercalation a) LEEM image (V_{st}= 5 V) of the surface b) Local spectra at the O *1s* core level from (A) non-intercalated regions and (B) the intercalated areas (B); for comparison the O *1s* spectrum from the intercalated region prior to the treatment is shown (thin red dotted line). c) Local spectra at the C *1s* core level (hν = 400 eV) from A and B regions.

The dispersion of the graphene band near its apex can be approximated as linear; therefore, the momentum width (extracted from the Lorentzian fit as described before) is proportional to the electronic scattering rate deriving from the many-body interactions such as electron-electron, electron-phonon and electron-defect scattering. The width of the graphene π band at the same E_D - E_B point (*i.e.* corresponding to an energy scale referred to the Dirac point) is smaller in the case of oxygen-intercalated graphene, thus confirming the similarity to a free-standing system (Fig. 3c). In addition, we notice that the experimentally determines values of FWHM and v_F are in good agreement with those obtained for oxygen intercalated graphene on Ni(111) [12]. Finally, the spectra acquired in normal emission, around the Γ point (Fig. 3e), show that the intensity of the Co *3d* bands is reduced upon O_2 intercalation. This effect is observed to be different for the two 3*d* bands (majority and minority spin). In fact, while the band present at E_B = 1.25 eV (majority-like) is almost fully attenuated, the intensity of the feature at 0.32 eV (minority-like) remains almost unaffected.

The abrupt change of the graphene band structure between the pristine and the intercalated regions is in agreement with the LEEM/XPEEM data. The existence of a sharp intercalation front allows one to have only two distinct types of regions. Therefore, no intermediate electronic configuration between these two states can be observed.

3.1. Reversibility of the process

Aiming to achieve a reversible modification of the electronic structure, we investigated the possibility of cycling the intercalation process by first removing the oxygen from the surface and then fully restoring the Gr layer in such a way that O_2 can be repeatedly intercalated. In the intercalated regions of the sample, we found that the oxygen removal takes place by annealing at T $\geq$ 380 °C. The LEEM image (Fig. 4a) shows that the deintercalation is locally associated with a structural change of the surface layer (region B), as highlighted by the presence of an inhomogeneous contrast. The O-free regions instead remain essentially unchanged by the treatment (region A).

In fact, previous studies have shown that the de-intercalation of oxygen is usually activated by UHV annealing in the range 280-330 °C [2, 12], but also at T up to 420 °C

[9]. Notably, in this temperature range, graphene etching is observed, and actually the graphene layer partially deteriorates due to carbon removal and defect formation. In the case of oxygen removal from the Gr/Ni(111) interface, severe damage of the graphene network is observed [1], while in the case of Ir(111), more than 50% of the initial graphene coverage is desorbed upon annealing of the intercalated graphene/metal interface [2].

XPEEM spectromicroscopy confirms that oxygen is removed from the intercalated regions, as indicated by the substantial reduction of the O *1s* intensity (Fig. 4b), with a residual quantity of about 2% with respect to the intercalated case. At the same time, we find that the C *1s* peak (Fig. 4c) shifts back to its original value (*i.e.* strongly interacting graphene on Co); with only a minor component at lower binding energies (E_B = 284.4 eV), which can be associated to the emission from the graphene atoms at the edges of the residual islands and/or atomic defects. The total C *1s* intensity, as determined by peak fitting, is 20% lower as compared to the O-free regions, indicating a deterioration of the carbon layer during the oxygen removal. In fact, the absence of atomic carbon fingerprint confirms that the carbon on the surface is still organized in graphene patches, meaning that there is no disgregation of graphene. Therefore, during desorption, oxygen partially recombines with the C atoms from the Gr. In the limiting case that no other channel for C removal is accessible, oxygen should desorb principally as CO and CO_2, while O_2 production should be much lower given the relative atomic density (O:C = 1:4). However, we note that in principle other channels for carbon removal are available in the temperature range used, such as bulk dissolution [26], and therefore the relative abundances of desorbing gasses could be different. The integrity of the graphene layer can be restored by CVD of C_2H_4, using the same conditions as for the preparation. Regrowth occurs only in the C-poor regions, whereas no 2^{nd} layer nucleation is found anywhere on the surface. Importantly, by this procedure the surface can be restored to its original state so that the full cycle can be in principle reiterated.

4. Conclusions

We exploited oxygen intercalation/de-intercalation as a method to reversibly switch the graphene coupling with the ferromagnetic substrate on and off. A real-time study of the intercalation reveals that the oxygen enrichment at the graphene/cobalt interface depends on the mutual epitaxial relation between graphene and the substrate and on the concentration of holes (carbidic islands) in the graphene layer. In the case of epitaxially oriented graphene, we demonstrated that the holes in the layer plays a fundamental role, acting as intercalation centers. This is also supported by the fact that independently from the rotational coherence of the graphene layer, the intercalation is strongly suppressed or absent when the holes are not present. The size and density of these islands, which can be controlled adjusting the T/p parameters during the graphene synthesis, are fundamental factors influencing both the intercalation kinetics and the extent of intercalated areas. In the final configuration, the concentration of oxygen in the intercalated areas corresponds to a surface coverage of a 0.5 ML. From the spectroscopical point of view, the presence of such amount of oxygen induces a chemical shift of the graphene C *1s* peak by 1.1 eV to lower binding energies. We have shown that the intercalation of the sample does not alter the oxidation state of the cobalt substrate and therefore its ferromagnetic character is preserved even after a saturated oxygen coverage at the graphene/metal interface. Moreover, it has been shown that the decoupling of graphene

from its support is reversible. This is obtained by first annealing above 380 °C the intercalated graphene/cobalt interface, allowing for oxygen removal, subsequently followed by the CVD graphene re-growth. This procedure allowed us to obtain a pristine graphene layer, which can be repeatedly subjected to intercalation.

Valence band mapping reveals that in the intercalated regions, the graphene band structure acquires a nearly free-standing character with slight p-doping, with the Dirac point found at 0.43 eV above the Fermi level. Moreover, the presence of oxygen leads to an increased Fermi velocity of the charge carriers with respect to the pristine case. The electronic decoupling has relevant consequences for the induced magnetism in graphene; in fact, after intercalation, the spin-polarized feature (minicone band) at the Fermi level disappears.

Considering the above listed facts, the ability to obtain a multiphased surface, composed both by intercalated and non-intercalated graphene, paves a way to functionalize the graphene/cobalt interface, since the regions with different electronic character coexist on the same surface.

Acknowledgments

Part of this work was carried out in the frame of the CERIC-ERIC internal project MAG-ALCHEMI.

Appendix A. Supplementary data

Supplementary data related to this article can be found at ...

References

[1] Y. Dedkov, W. Klesse, A. Becker, F. Späth, C. Papp, E. Voloshina, Decoupling of graphene from Ni(111) via formation of an interfacial NiO layer, Carbon 121 (2017) 10–16.
[2] R. Larciprete, et al., Oxygen switching of the epitaxial graphene-metal interaction, ACS Nano 6 (2012) 9551–9558.
[3] T. Li, J. A. Yarmoff, Intercalation and desorption of oxygen between graphene and Ru(0001) studied with helium ion scattering, Physical Review B 96 (2017) 155441.
[4] E. Granas, et al., Oxygen intercalation under graphene on Ir(111): energetics, kinetics, and the role of graphene edges, ACS Nano 6 (2012) 9951–9963.
[5] H. Li, J. Xiao, Q. Fu, X. Bao, Confined catalysis under two-dimensional materials, Proceedings of the National Academy of Sciences 114 (2017) 5930–5934.
[6] M. Chen, R. C. Haddon, R. Yan, E. Bekyarova, Advances in transferring chemical vapour deposition graphene: A review, Materials Horizons 4 (2017) 1054–1063.
[7] L. Ma, X. C. Zeng, J. Wang, Oxygen intercalation of graphene on transition metal substrate: an edge-limited mechanism, The journal of physical chemistry letters 6 (2015) 4099–4105.
[8] P. Sutter, J. T. Sadowski, E. A. Sutter, Chemistry under cover: tuning metal-graphene interaction by reactive intercalation, Journal of the American Chemical Society 132 (2010) 8175–8179.
[9] R. Blume, et al., The influence of intercalated oxygen on the properties of graphene on polycrystalline Cu under various environmental conditions, Physical Chemistry Chemical Physics 16 (2014) 25989–26003.
[10] Q. Fu, X. Bao, Surface chemistry and catalysis confined under two-dimensional materials, Chemical Society Reviews 46 (2017) 1842–1874.
[11] R. Mu, et al., Visualizing chemical reactions confined under graphene, Angewandte Chemie International Edition 51 (2012) 4856–4859.

[12] L. Bignardi, et al., Key role of rotated domains in oxygen intercalation at graphene on Ni(111), 2D Materials 1 (2017) 025002.
[13] D. Marchenko, et al., Highly spin-polarized Dirac fermions at the graphene/Co interface, Physical Review B 91 (2015) 235431.
[14] D. Usachov, et al., Observation of single-spin dirac fermions at the graphene/ferromagnet interface, Nano Lett. 15 (2015) 2396–2401.
[15] Y. S. Dedkov, M. Fonin, Electronic and magnetic properties of the graphene-ferromagnet interface, New Journal of Physics 12 (2010) 125004.
[16] A. Varykhalov, et al., Intact dirac cones at broken sublattice symmetry: Photoemission study of graphene on ni and co, Phys. Rev. X 2 (2012) 041017.
[17] A. Varykhalov, O. Rader, Graphene grown on co(0001) films and islands: Electronic structure and its precise magnetization dependence, Phys. Rev. B 80 (2009) 035437.
[18] A. D. Vu, et al., Unconventional magnetisation texture in graphene/cobalt hybrids, Sci. Rep. 6 (2016) 24783.
[19] H. Yang, et al., Anatomy and giant enhancement of the perpendicular magnetic anisotropy of cobalt-graphene heterostructures, Nano Lett. 16 (2016) 145–151.
[20] F. Genuzio, P. Genoni, T. O. Mente, B. Santos, A. Sala, C. Lenardi, A. Locatelli, Stimulated CO Dissociation and Surface Graphitization by Microfocused X-ray and Electron Beams, The Journal of Physical Chemistry C 123 (2019) 8360–8369.
[21] F. Ajejas, et al., Unraveling dzyaloshinskii-moriya interaction and chiral nature of graphene/cobalt interface, Nano Lett. 18 (2018) 5364–5372.
[22] H. Yang, et al., Significant Dzyaloshinskii-Moriya interaction at graphene-ferromagnet interfaces due to the Rashba effect, Nature Materials 17 (2018) 605–609.
[23] D. Y. Usachov, et al., Raman spectroscopy of lattice-matched graphene on strongly interacting metal surfaces, ACS Nano 11 (2017) 6336–6345.
[24] T. Menteş, G. Zamborlini, A. Sala, A. Locatelli, Cathode lens spectromicroscopy: Methodology and applications, Beilstein J. Nanotechnol. 5 (2014) 1873–1886.
[25] C. Wiemann, et al., A new nanospectroscopy tool with synchrotron radiation: NanoESCA@Elettra, e-Journal of Surface Science and Nanotechnology 9 (2011) 395–399.
[26] M. Jugovac, et al., Role of carbon dissolution and recondensation in graphene epitaxial alignment on cobalt, Carbon 152 (2019) 489 – 496.
[27] D. Usachov, et al., Cobalt-assisted recrystallization and alignment of pure and doped graphene, Nanoscale 10 (2018) 12123–12132.
[28] S. Vlaic, N. Rougemaille, A. Kimouche, B. S. Burgos, A. Locatelli, J. Coraux, Intercalating cobalt between graphene and iridium (111): Spatially dependent kinetics from the edges, Physical Review Materials 1 (2017) 053406.
[29] S. C. Petitto, E. M. Marsh, G. A. Carson, M. A. Langell, Cobalt oxide surface chemistry: The interaction of CoO(100), Co_3O_4(110) and Co_3O_4(111) with oxygen and water, Journal of Molecular Catalysis A: Chemical 281 (2008) 49–58.
[30] M. C. Biesinger, et al., Resolving surface chemical states in XPS analysis of first row transition metals, oxides and hydroxides: Cr, Mn, Fe, Co and Ni, Applied Surface Science 257 (2011) 2717–2730.
[31] S. Sahu, G. Rout, Band gap opening in graphene: a short theoretical study, International Nano Letters 7 (2017) 81–89.
[32] S. Ma, Z. Jiao, T. Wang, X. Dai, First-principles studies of oxygen chemisorption on Co(0001), Surface Science 619 (2014) 90–97.
[33] S. Ulstrup, P. Lacovig, F. Orlando, D. Lizzit, L. Bignardi, M. Dalmiglio, M. Bianchi, F. Mazzola, A. Baraldi, R. Larciprete, P. Hofmann, S. Lizzit, Photoemission investigation of oxygen intercalated epitaxial graphene on Ru(0001), Surface Science 678 (2018) 57 – 64. Surface Structure and Dynamics in Honor of Karl-Heinz Rieder.
[34] B. T. Thole, P. Carra, F. Sette, G. van der Laan, X-ray circular dichroism as a probe of orbital magnetization, Physical Review Letters 68 (1992) 1943–1946.
[35] P. Carra, B. T. Thole, M. Altarelli, X. Wang, X-ray circular dichroism and local magnetic fields, Physical Review Letters 70 (1993) 694–697.
[36] H. Vita, S. Böttcher, P. Leicht, K. Horn, A. B. Shick, F. Máca, Electronic structure and magnetic properties of cobalt intercalated in graphene on Ir(111), Physical Review B 90 (2014) 165432.
[37] E. Voloshina, N. Berdunov, Y. Dedkov, Restoring a nearly free-standing character of graphene on Ru(0001) by oxygen intercalation, Scientific Reports 6 (2016) 20285.
[38] S. Ulstrup, M. Andersen, M. Bianchi, L. Barreto, B. Hammer, L. Hornekr, P. Hofmann, Sequential

oxygen and alkali intercalation of epitaxial graphene on Ir(111): enhanced many-body effects and formation of pn-interfaces, 2D Materials 4 (2014) 025106.
[39] C. Romero-Muiz, A. Martn-Recio, P. Pou, J. M. Gmez-Rodrguez, R. Prez, Strong dependence of flattening and decoupling of graphene on metals on the local distribution of intercalated oxygen atoms, Carbon 101 (2016) 129 – 134.
[40] D. Elias, et al., Dirac cones reshaped by interaction effects in suspended graphene, Nature Physics 7 (2011) 701.